Journal of Molecular Graphics and Modelling 29 (2010) 461–469

Contents lists available at ScienceDirect

Journal of Molecular Graphics and Modelling

journal homepage: www.elsevier.com/locate/JMGM

Computational analysis of water residence on ceramide and sphingomyelin bilayer membranes

Yosuke Imai, Xinli Liu, Junya Yamagishi, Kenichi Mori, Saburo Neya, Tyuji Hoshino*

Graduate School of Pharmaceutical Sciences, Chiba University, 1-33 Yayoi-cho, Inage-ku, Chiba 263-8522, Japan

ARTICLE INFO

Article history:
Received 21 July 2010
Received in revised form 8 September 2010
Accepted 14 September 2010
Available online 18 September 2010

Keywords:
Water residence time
Lipid membrane
Distribution function
Hydration shell
Molecular dynamics simulation

ABSTRACT

Many physical chemical properties of lipid membranes, for example, the thickness, phase state, order parameter, and fluidity, can be understood straightforwardly. Water residence on a membrane is, however, an exception. To tackle this problem, we have performed molecular dynamics simulations of the distribution of water normal to the surface of several lipid membranes and from this deduced the associated water residence time. Our analysis of the results clearly indicates that lipid membranes have hydration shells on their surface, just as a solute in an aqueous solution does, and that the water residence time can be estimated from the potential for the mean force field derived from the distribution function of the water. We have done this atomic-scale analysis for ceramide bilayers and contrasted the calculation results with those for sphigomyelin bilayers, revealing that sphingomyelin bilayers can retain water molecules longer than ceramide bilayers and that the total number of water molecules retained on the membrane surface of sphingomyelin is larger than that for ceramide. In addition, we find that not only polar atoms of lipid molecules, such as oxygen, but also non-polar atoms, such as carbon, influence the motion of water on the membranes.

© 2010 Elsevier Inc. All rights reserved.

1. Introduction

Molecular dynamics (MD) simulation is one of the most popular theoretical approaches to analyzing biological phenomena at an atomic level. Recently, many simulation studies have been performed on biomembranes with lipid bilayers [1,2] and on the proteins inside the lipids [3]. For example, Pandit and Scott performed a pioneering work of MD simulation for ceramide bilayers, introducing order parameters and electron density profiles among other characterizations [4]. Other groups have carried out simulations on phospholipids [5] or mixed membranes [6]. Recently, computational techniques for analyzing interactions between proteins and lipid membranes have been improved to stably simulate more complex model systems such as a protein embedded in a mixed membrane or a protein attached to a membrane surface [7–9]. Our understanding of the functioning of biomembranes at the atomic scale should rapidly advance with the assistance of these new techniques in computational biology, but only with concomitant advances in accurate interpretation of experimental data [10] and its extrapolation to the reliable prediction of biological phenomena.

In this paper, we present an analytic technique based on MD simulation for estimating the residence time of water on different kinds of membranes, i.e., how long water molecules stay on a membrane. In computational studies, the radial distribution function (RDF) is sometimes employed to describe the behavior of water with respect to a particular atom [11–13], and the concerted, long-term efforts of many researchers have made computational techniques for estimating the water residence time robust [14,15]. A recent study successfully estimated the residence time of water in a solute hydration shell [16]. Unfortunately, the RDF cannot be applied to water on a membrane because water molecules on a membrane are not distributed spherically. Instead, our present approach attempts to simulate particle distribution above a plane rather than about a point, and, from the simulated distribution of water on a planar membrane, we calculate the residence time of the water.

Lipid molecules are classified into three families: phospholipid, sphingolipid, and cholesterol. Ceramides belong to the sphingolipid family with a basic backbone of glycosphingolipid but without any functional head groups such as sugar rings or phosphocholines. Ceramides are known to play important roles in both intra- and inter-cellular communication [17], and have attracted much recent attention because they might be incorporated into micro-domains called rafts which are highly ordered but have some degree of fluidity [18–20] and serve as second messengers in cell differentiation and the death process apoptosis [21–23].

* Corresponding author. Tel.: +81 43 290 2926; fax: +81 43 290 2925.
E-mail address: hoshino@faculty.chiba-u.jp (T. Hoshino).

1093-3263/$ – see front matter © 2010 Elsevier Inc. All rights reserved.
doi:10.1016/j.jmgm.2010.09.002

Table 1
Thickness, area per lipid, and gauche ratio of the equilibrated lipid bilayers.

	12:0	14:0	16:0	18:0	20:0	18:1
Ceramide						
Thickness (Å)	33.7 ± 0.5	40.7 ± 0.3	41.6 ± 0.9	42.0 ± 0.4	43.3 ± 0.4	35.0 ± 0.6
Area per lipid (Å^2)	46.3 ± 0.8	41.6 ± 0.3	42.5 ± 0.5	44.8 ± 0.5	44.1 ± 0.4	54.9 ± 1.4
Gauche ratio	15.7	7.2	8.7	10.0	13.1	29.5
Sphingomyelin						
Thickness (Å)	34.8 ± 0.6	38.5 ± 0.4	38.4 ± 0.5	41.9 ± 0.8	36.1 ± 0.3	37.9 ± 0.8
Area per lipid (Å^2)	56.8 ± 1.2	53.3 ± 0.6	57.1 ± 1.0	53.8 ± 1.3	64.8 ± 0.6	61.5 ± 1.6
Gauche ratio	23.2	23.9	19.7	25.8	16.3	28.6

Ceramides are abundant in skin. A unique periodic structure, lipid lamella, is observed in the stratum corneum, the outermost layer of skin. Patients with atopic dermatitis have a shortage of ceramide in the stratum corneum, perhaps causing a degradation of the barrier function of skin [24–26]. Another critical role of skin is to keep moisturizing. Ceramide are main component of lipid lamella and detected at the rate of about 50%. The affinity to waters is one of the important properties of lipid membranes. However, the behavior of waters or the water residence time on a membrane surface has been not closely studies in the field of theoretical calculation so far.

Many approaches have been developed to measure the physical chemical properties of ceramides and their analogues. For example, Fourier transform infrared (FTIR) spectroscopy and differential scanning calorimetry (DSC) have shown that the phase transition temperature (T_m) between gel and liquid-crystal phases is 93 ± 1 °C and that this temperature varies with the chain length of the tail group [27].

In our study, six different kinds of membranes with ceramide bilayers are modeled with different length carbon chains of the acyl group: 12:0, 14:0, 16:0, 18:0, 20:0, and 18:1. In the format of #A:#B for lipid molecules, #A represents the length of carbon chain and #B indicates the number of unsaturated bonds. The backbones of these acyl chains are derived from lauric, myristic, palmitic, stearic, arachidic, and oleic acid, respectively, which are free fatty acids in our body. We carried out modeling of the ceramide membranes, MD simulations, analysis of the simulation results, observation of common features of the ceramides, and estimation of the residence time of water.

As pointed out by Li et al. [28], the structure of the hydrophilic head groups of lipids is important in water retention. Hence, simulation and analysis were performed on the membranes with different types of head groups for comparison. Sphingomyelins were selected for this purpose because sphingomyelins have the same acyl chain structure as ceramides and differ only in the structure of the head group [29].

2. Method

2.1. Modeling of membranes

VMD [30] was used to make a model of a POPC bilayer that has 30 POPC molecules per half leaflet, i.e., 60 molecules in a bilayer in total. The POPC molecules were then converted into ceramide (Cer) or sphingomyelin (SM) by modifying the POPC head and tail groups. Thus we acquired 12 Cer or SM bilayer models composed of single molecular species in which the length of the carbon chain is 12:0, 14:0, 16:0, 18:0, 20:0 or 18:1. An unsaturated bond in the acyl group for the 18:1 model has a *cis* conformation and is located between 9 C and 10 C. The TIP3P explicit water model [31] was used to solvate each membrane system to a thickness of 40 Å above and below the bilayer. Sodium and chloride ions were added in the water layers at a concentration of 0.15 mol/L.

2.2. MD simulation

The NAMD simulation package [32] was employed to perform all the processes of simulation. Energy minimization was initially carried out for 10,000 steps to release strain due to steric hindrance. Next, the model system was heated to 310 K for 6000 steps. Simulations for equilibration were then carried out under the NPT ensemble condition at a temperature of 310 K and an isotropic pressure of 1 atm. The head groups of the lipids were under the harmonic constraint at this initial stage to maintain the bilayer structure of the membrane. The simulation was executed for 2 ns while the constraints were weakened gradually and a subsequent 2 ns under no constraints. Finally, 20-ns simulations for the Cer models and 10-ns simulations for the SM models were executed as production runs.

CHARMM 27 parameters [33] were adopted for the EM force field of the lipids and CHARMM 22 [34] for the others. The long-range electrostatic interaction was calculated at every step with the particle mesh Ewald (PME) method under periodic boundary conditions [35]. The integration time step was set to 2 fs. All the covalent bonds connecting to hydrogen atoms were constrained by the SHAKE algorithm or the SETTLE method for the water [36,37]. The Langevin thermostat method was employed to control the temperature [38]. Short-range non-bonded interactions were cut off smoothly between 10 and 12 Å.

2.3. Analysis

All the results shown in Tables 1 and 2 were produced by analysis of the MD simulation for the last 5 ns of the production runs using 500 snapshots of the structures, one acquired every 0.01 ns. The thickness is extracted from the distances between the oxygen atoms of the hydroxyl group for Cer and the phosphorus atoms of the phosphate group for SM. The area per lipid is obtained by dividing the area in the of x–y plane of the unit cell by the number of lipid molecules in the half leaflet. The deuterium order parameter, indicating the degree of ordering of the lipids, is calculated from the equation.

$$S_{CD} = \frac{1}{2}\left|3\left\langle \cos^2\theta \right\rangle - 1\right| \quad (1)$$

where θ represents the average angle between the normal vector of the membrane's surface and the vector of the C–H bond of the CH_2 group of the lipids. The brackets denote an average over time and over all the lipids.

The radial distribution function (RDF) is usually applied to describe how many objective particles exist around a particular

Table 2
Residence time of water on the bilayer membranes.

	12:0	14:0	16:0	18:0	20:0	18:1
Ceramide (ps)	6.00	6.48	6.46	5.64	5.72	5.38
Sphingomyelin (ps)	8.49	8.94	8.75	8.63	8.14	7.96

particle. The RDF of objective particles in a space is derived from the equation:

$$g(r) = \frac{n(r)}{4\pi r^2 \Delta r} \times \frac{1}{\rho} \quad (2)$$

where r represents the distance from a particular particle, $n(r)$ represents the number of objective particles between r and $r + \Delta r$, and ρ represents the density of objective particles for infinite separation from the particular particle. We modified this equation to be applicable to objective particles on a surface with r representing the distance along the surface normal measured from the center of the bilayer and $n'(r)$ denoting the number of objective particles per unit area:

$$g(r) = \frac{n'(r)}{\Delta r} \times \frac{1}{\rho} \quad (3)$$

Fig. S1 in Supplementary Data shows the scheme for calculating $n'(r)$ of water that is distributed from the membrane's surface to the bulk water layer. The distance between each water molecule and the lipid atom closest to the water molecule is calculated and is presented as a histogram. This histogram shows the distribution of water molecules when the positions of all the closest lipid atoms are settled at the top surface (x–y plane) and all water molecules are at the distance r along the direction normal to the membrane (z axis). Thus the acquired plot represents how many water molecules exist at a particular distance from the surface. For example, the plot has a peak at the distance for hydrogen bonding.

The residence time for water molecules on the membrane surface was roughly estimated from the formalism described by Laage and Hynes [16]:

$$\tau = \frac{1}{k_f}[1 + k_b t^* + k_b(k_f - k_d)t^{*2} + o(t^*)^2] \quad (4)$$

The rate constants, k_f, k_b, and k_d, correspond to the forward and reverse reactions between the first and second hydration layers and the dissociation reaction from the second hydration layer to the bulk. These rate constants were determined from the equation:

$$k = A \exp\left(\frac{\Delta E}{k_B T}\right) \quad (5)$$

where $\triangle E$ is the energy barrier for the respective reactions estimated from the potential for the mean force field deduced from the distribution function $g(r)$. The pre-exponential factor A was postulated the same for k_f, k_b, and k_d, and set to 0.7×10^{12}, based on the water residence time around an ion [16]. The tolerance time t^* was set to 2 ps.

3. Results

3.1. Structural property

Top and side views of six kinds of ceramide bilayers after 20-ns MD simulations are shown in Fig. 1. The structures obtained differ among the bilayers, despite the atomic geometries in the head groups being similar to each other initially, so this difference must be a consequence of the effect of hydrophobic interaction due to the difference in length of the carbon chains of the tail group. The five ceramide bilayers with the saturated acyl chain seem to form a gel phase, while the ceramide bilayer with the unsaturated acyl group forms a liquid crystal phase. The critical temperature (T_m) for the gel-liquid crystal phase transition is known to be approximately 90 °C for the saturated ceramide bilayers [27], and the T_m varies with the length of the carbon chain. The simulations reported here were executed at 310 K, and all the saturated ceramides in Fig. 1 show a gel phase. Accordingly, the final simulated phase state is compatible with the experimental findings.

A few ceramide molecules are observed to diffuse into the 12:0 ceramide bilayer membrane because of the weakness of the carbon chain packing (see the 12:0 ceramide in Fig. 1, note the middle of the side view). On the other hand, most of the carbon chains are regularly aligned and the terminal carbon atoms are well-ordered for the 14:0 ceramide membrane, forming a stable and rigid bilayer structure. For the 16:0 ceramide, the increased number of carbon atoms in the acyl group makes the lipids more hydrophobic, leading to the formation of a highly-ordered lipid bilayer compared to the 12:0 ceramide, despite the difference in the length between the carbon chain of the acyl group and that of the sphingosine backbone being the same for the two species. The 18:0 ceramide has a few molecules partially diffused into the membrane, which can only rarely escape from the inside of the membrane because highly-ordered lipids surround them. The 20:0 ceramide bilayer has a difference of six carbon atoms in length between the acyl group and the sphingosine backbone, causing a unique wavy structure similar to a Pβ' phase and distorting the membrane. The 18:1 ceramide bilayer is seen to form a liquid crystalline phase (Pα) as a result of disordering at the middle of the acyl group due to the *cis* configuration of the unsaturated bond.

Some fundamental analyses on the lipid membranes were performed and the thickness, area per lipid, and gauche ratio summarized in Table 1. A plot of the order parameter along the carbon chain is presented in Fig. S2. The changes in the thickness and area per lipid during the last 10 ns are also shown in Figs. S3 and S4. All the results in Table 1 were obtained by sampling the structure every 10 ps for the last 5 ns and averaging the values over 500 snapshot structures. These data quantitatively support the findings described in the above paragraph. In the 14:0 ceramide, the population of the carbon atoms maintaining the gauche conformation, the so-called gauche ratio, is low, which means almost all the carbon chains are aligned along the z axis. On the other hand, there appears to be some disorder in the middle of the lipid bilayer for the other kinds of ceramides. Since one of the two carbon chains of the tail group is longer than the other, a few molecules are likely to move along the z axis or cause the membrane to be wavy.

These results are also reflected in the values for the membrane thickness and area per lipid. The thickness for the 14:0 ceramide is much larger than that for the other membranes because of the highly ordered alignment of its carbon chains. This alignment leads to the close packing of the ceramide molecules and the low values for the area per lipid. In contrast, the gauche ratio is quite high for the ceramide with unsaturated acyl chains (18:1) and the chains are disordered. This disorder leads to low membrane thickness and high area per lipid values.

The gauche ratio acquired from infrared measurements is generally used as a standard index, the ratio being low for an ordered gel phase and high for a disordered liquid crystalline phase. The gauche ratios in Table 1 were measured following Zaraiskaya and Jeffrey [39]. The values of the order parameter in Fig. S2 in the plateau region are similar among the 14:0, 16:0, 18:0, and 20:0 ceramides. The 12:0 ceramide has a relatively low hydrophobicity and weak packing property owing to the shortness of the carbon chains, which is reflected in the low values for the order parameter. In the 14:0 ceramide, the orderings of the two carbon chains are almost equal because the carbon chain lengths are the same.

3.2. Water residence on membranes

The RDF is often used to measure the ability of metals or ions to retain water. It represents the relative density distribution of objective particles (e.g., water molecules) surrounding a particular particle (e.g., an ion or molecule of metal). Instead of using the RDF, we constructed a DF of objective particles above a plane. Using the simple algorithm shown in Fig. S1, we have successfully obtained

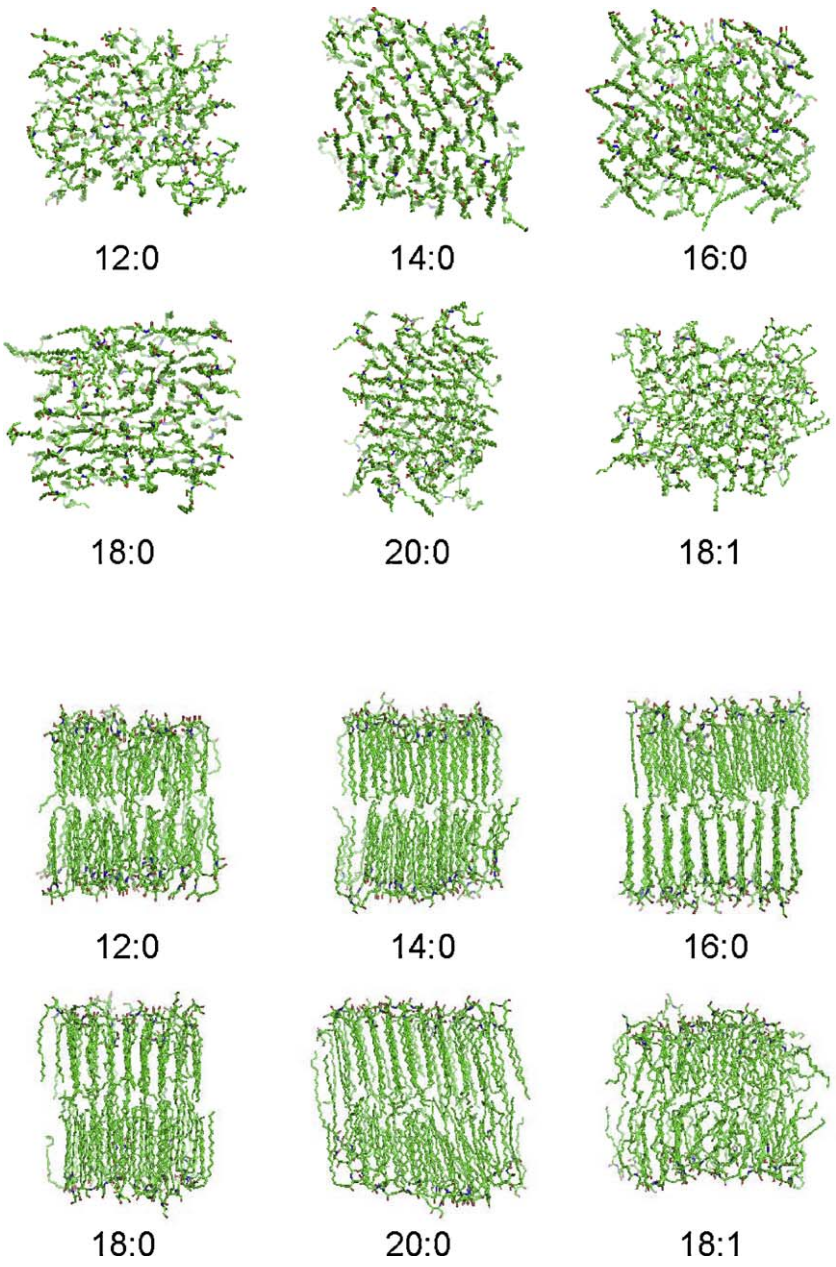

Fig. 1. Snapshots of structure of the ceramide lipid bilayers obtained after 20-ns production runs of the MD simulation. (upper) top view. (lower) Side view. Oxygen, nitrogen, and carbon atoms are red, blue, and green, respectively. Hydrogen atoms and solvents are not shown for clarity. (For interpretation of the references to color in this figure legend, the reader is referred to the web version of the article.)

the DF of water on a biomembrane. In biomembranes, the transient layer extending from the lipids to the bulk water is in the range of 2–5 Å in thickness. While the RDF of objective atoms around a particular atom usually has first and second hydration peaks, the DF for a membrane gives a large first maximum and a small shoulder-like peak after the first maximum, followed by a shallow minimum and a slight second hydration peak. The density of water molecules becomes constant far away from the membrane, so water 10 Å beyond the membrane surface is regarded as bulk water (Fig. 2).

Detailed observation of the results of the simulations reveals that most of the water molecules clustered at the first maximum of the DF are close to oxygen atoms of the ceramide lipids at a distance of 2.7–2.8 Å from the closest lipid oxygen atom, as shown in Fig. 3(a). That is, this peak corresponds to hydrogen bonding of the water molecules with oxygen atoms of the ceramide lipid molecules with the position of the peak matching the hydrogen bond length. For water molecules for the small shoulder peak at 3.5–3.6 Å, more than half of the atoms in the lipids closest to the water are carbon atoms, as shown in Fig. 3(b). Accordingly, we decomposed the DF into two parts in Fig. 2: the blue curve for water molecules closer to the lipid oxygen atoms and the red curve for those closer to the lipid carbon atoms. For all the ceramide bilayers, almost all the water molecules at the first maximum are close to lipid oxygen atoms, and those at the shoulder peak are confirmed to be close to lipid carbon atoms. Note also that the average distance between the water molecules and the carbon atoms is different from that between the water molecules and the lipid oxygen atoms, the difference becoming more prominent when the membrane becomes more disordered. Further, the DF of the 18:1 ceramide has a large shoulder peak.

From the calculated DF, we obtained the potential for the mean force field in Fig. S5 and then estimated the residence time of water

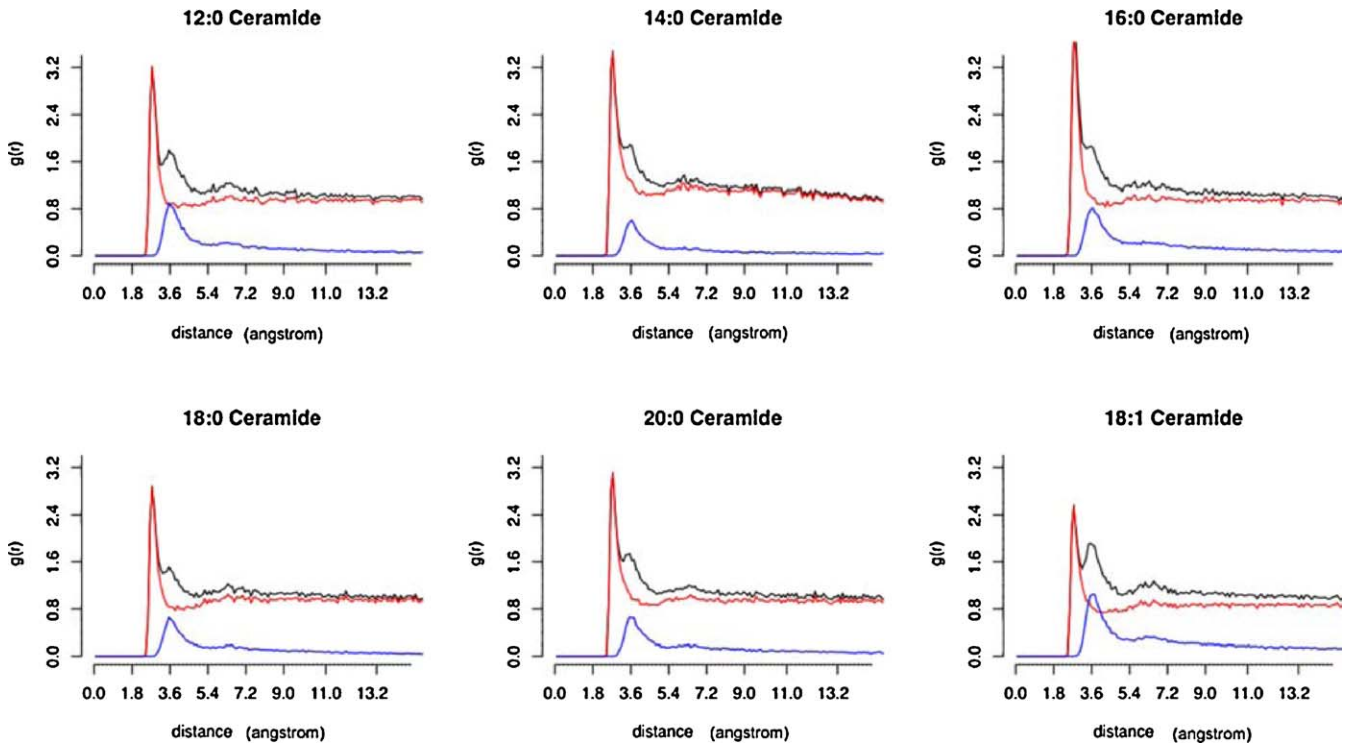

Fig. 2. Distribution function of water molecules on the ceramide membranes. This distribution function (black) is decomposed into two components. One is for the water molecules whose closest lipid atom is oxygen (red), and the other is for the water whose closest lipid atom is carbon (blue).

on the membrane's surface, as shown in Table 2. The estimation indicates that it takes about 6 ps for one water molecule on the membrane to transfer to the bulk water layer. Interestingly, the water residence times are quite similar among the ceramides with relatively short carbon chains while the time is a little bit smaller for the ceramide with longer, unsaturated acyl groups.

3.3. Sphingomyelin bilayer

We performed similar calculations for membranes with sphingomyelin bilayers and measured the thickness, area per lipid, and gauche ratio, and then deduced the DF for water to estimate the residence time of water given in Tables 1 and 2 (see also Figs. S6–S9). The side views for the membranes with sphingomyelin in Fig. 4 show that the carbon chains are slightly disordered for the 12:0, 14:0, 16:0, and 18:0 membranes. Due to the difference in length of the two carbon chains of sphingomyelin, most of the acyl chains in both leaflets are inclined from the surface normal direction. This inclination is reflected in the large gauche ratio of the 18:0 membrane in Table 1. For the membrane with 20:0 sphingomyelin, the carbon chains from both leaflets are interdigited in the middle of the bilayer. The effect of the interdigitation is clearly reflected in the decrease of the membrane's thickness, the prominent increase of the area per lipid, and the reduction of the gauche ratio in Table 1. The side view for the membrane with the unsaturated acyl group (18:1) shows that the carbon chains are considerably disordered. This disorder causes an increase of the gauche ratio and results in a small membrane thickness and large area per lipid.

The DFs for the sphingomyelin bilayers in Fig. 5 show noticeable differences from those of the ceramides. The height of the first maximum is 4.8–5.2 Å in the sphingomyelins and 2.6–3.5 Å in the ceramides. This means that a sphingomyelin bilayer can attract more water molecules on its surface than a ceramide bilayer. This finding can be straightforwardly understood from the number of donor and acceptor atoms for hydrogen bonding, such as the oxygen atom of the phosphate group. There are many more water molecules at the shoulder peak around 3 Å for the sphingomyelin bilayers than for the shoulder peak for the ceramide bilayers. This peak is mainly derived from the water molecules whose closest lipid atom is carbon. Most of the water molecules are located not at the bottom part of the head group of the lipids, as in case of the ceramides, but at the choline group of the head group. Due to the positions of the carbon atoms in the head group, the two peaks overlap each other in the DFs for the sphingomyelin bilayers. The residence time of water on the sphingomyelin bilayer has been estimated to be 8–9 ps, based on the potential for the mean force field in Fig. S9 obtained from Fig. 5. The residence times for the sphingomyelins are longer than those for the ceramides. Evidently, the structure of the head group of the lipids indeed affects the residence time of water.

4. Discussion

4.1. Water distribution function on membranes

In our theoretical approach, it is very important how to obtain the DF of water on the membrane. We first tried to calculate the density of water along the z axis by counting the number of water molecules in dz as shown in Fig. S1(a′). The intended DF should have been acquired when this data was scaled by the number density of water molecules at an infinite separation from the membrane. However, a plot of this DF did not have any peak because it was washed out by averaging over a non-planar surface generated by easily moving moieties on the membrane. In other words, a simple count of the number of water molecules along the z axis could not accurately reflect the topology of the membrane–water interface. The standard deviation of roughness of the membrane surface is 2–3 Å for ceramide and 2–4 Å for the sphingomyelin bilayers.

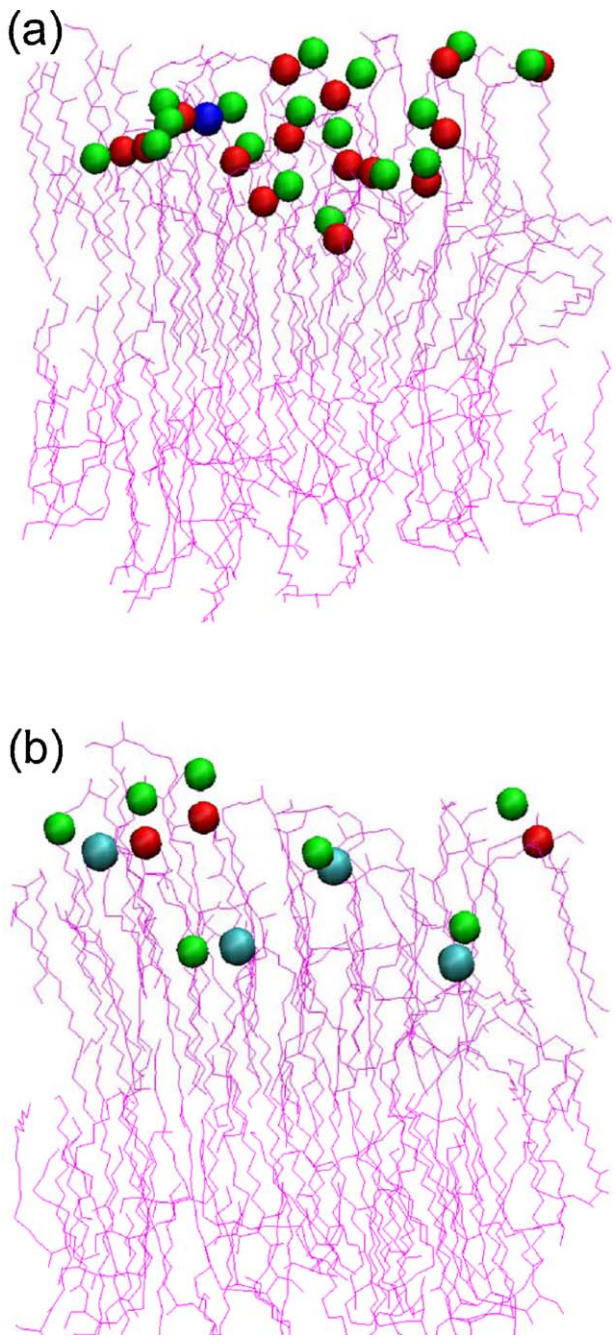

Fig. 3. Location of the water molecules corresponding to the first maximum (a) and the second shoulder peak (b) in the distribution function, exemplified from the snapshot structure of the 20:0 ceramide membrane after a 20-ns MD simulation. The positions of oxygen atoms of the water molecules are represented by green spheres. The closest lipid atoms of the water molecules are denoted by red (oxygen) or cyan (carbon) spheres. Remaining parts of the lipid molecules are depicted by magenta lines. (For interpretation of the references to color in this figure legend, the reader is referred to the web version of the article.)

These values are of the order of the thickness of the transient layer of water, about 2.5 Å. This transient layer is the first hydration layer which we intended to measure. Therefore, we employed an alternative algorithm for estimating the DF by focusing on the distance between a water molecule and its closest lipid, as in Fig. S1(a).

As shown in Fig. 3, the closest atoms to the water molecules are not only the lipid oxygen atoms. The decomposition of the DF of water on membrane in Fig. 2 reveals that not only oxygen but also carbon is involved in the movement of water molecules above the membrane. Surprisingly, the DF of water molecules above the membrane with respect to the closest lipid carbon atoms has a peak. The $g(r)$ of water molecules whose closest atoms are oxygen shows clear first and second hydration peaks with a shallow minimum between them. On the other hand, the $g(r)$ for water whose closest atoms are carbon only has a shallow minimum. This implies that the water molecules whose closest atoms are oxygen form some ordered network propagating from the membrane, and that, in contrast, the water molecules whose closest atoms are carbon are disordered and form no such network.

4.2. Water residence time

Recent progress, both in theory and experiment, has shed light on the residence time for water in the first hydration shell around an ion. A theoretical study estimated the water residence time in a hydration shell around a chloride ion to be 5–12 ps [16]. Moilanen et al. successfully observed ion–water hydrogen bond switching using two-dimensional vibrational echo chemical exchange spectroscopy [40,41]. They studied the behavior of water molecules interacting with a tetrafluoroborate (BF_4^-) ion. The time scale for a hydrogen bond to switch from the ion to a water molecule was estimated to be about 7 ps. This switching time of 7 ps is representative of the residence time of water in the hydration shell of anions in dilute solutions. It is plausible that the residence time of water on a membrane is close to the timescale reported for water exchange around ions, and indeed the residence time of water on the membranes was estimated from our simulations to be about 6 ps for the ceramides and 8 ps for the sphingomyelins.

The distribution function of water molecules; $g(r)$ in Eq. (3), was obtained, using all the acquired 500 snapshot structures, because $g(r)$ is a function of distance r and a fine histogram with r is scarcely obtained from only one snapshot. It will be important to estimate the deviation of $g(r)$ among snapshot structures. The $g(r)$ value at the first maximum peak and its standard deviation are shown in Table S1 of Supplementary Data. Since the differences in averaged $g(r)$ maximum values among lipid bilayers are comparable to the standard deviations, the difference in distribution function for water is statistically significant.

It is informative to examine how the structure of the membranes and differences in the lipid species affect the water residence time by comparing the DFs and water residence times among the ceramide and sphingomyelin bilayers. Water molecules stay on the sphingomyelin bilayers about 2 ps longer than on the ceramides, given lipids with the same carbon chain length. This reproducibility clearly suggests that a sphingomyelin bilayer has a larger capacity for retaining water than does a ceramide. Remarkably, a comparison between Figs. 2 and 5 indicates that the number density at the shoulder peak is much higher in the sphingomyelin bilayers than for the ceramides. Water molecules can be held by the choline group in the sphingomyelin but not in the ceramide. Also the length of the acyl chain of the lipids affects the water residence time. With a decrease in the difference between the carbon chain length of the sphingosine backbone and that of the acyl group, the membrane is likely to retain water longer; i.e., the capacity to retain water near the carbon atoms appears to be enhanced with a decrease of the imbalance in length of the two carbon chains.

These findings suggest the importance of the molecular structure of a membrane's surface for water residence. The membrane surface has a structure like a cave with several polar atoms located at the entrance of the cave. Some water molecules are trapped inside the cave, and the closest lipid atom to those waters is carbon. In sphingomyelin, the large polar chemical groups cover the entrance of the cave. Accordingly, the trapped water molecules cannot rapidly be exchanged with water molecules from the outer region.

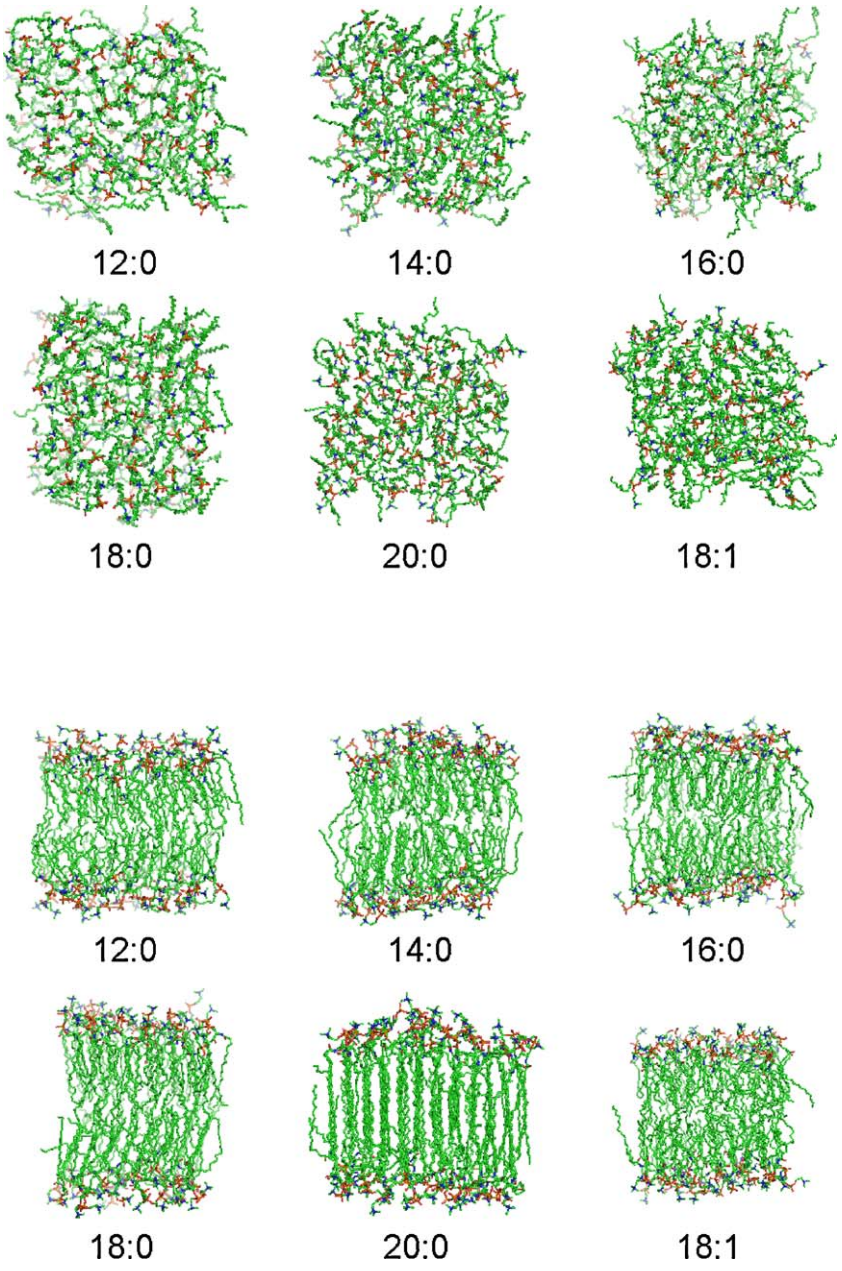

Fig. 4. Snapshot structure of sphingomyelin lipid bilayers. (upper) Top view. (lower) Side view. Oxygen, nitrogen, and carbon atoms are denoted by red, blue, and green, respectively. Hydrogen atoms and solvent waters are not shown for clarity. (For interpretation of the references to color in this figure legend, the reader is referred to the web version of the article.)

4.3. Model size and time scale of the simulation

A model system of proper size must be constructed when conducting molecular dynamics simulations. Chiu et al. modeled a large sphingomyelin bilayer whose side length was 400 nm to reproduce a lipid raft and ran 3.8-ns simulations [42]. The model system for our work was designed to be smaller to make the calculations easier and to allow us to focus on the motion of water molecules.

Lipids have several motions, such as rotation, intrusion, stretching, lateral diffusion, ruffling, and flip-flop. The small model systems used in this work cannot represent the ruffling and flip-flop motion. However, according to the reports by Padit et al. [6] and other groups [43,44], the ruffling mode of action seems not to appear in a membrane with only a single lipid species. Moreover, a large ruffling motion that causes the wrapping of many water molecules by the membrane has not been reported. Accordingly, we have neglected any ruffling motion. The timescale of the flip-flop mode, with a frequency of about 1 ms^{-1}, is very different from that of the phenomena we have considered. Therefore, flip-flop was also neglected. Thus, the model systems used in this work are small but adequate to include rotation, intrusion, stretch, and lateral diffusion of lipids by incorporating a sufficiently thick water layer.

The simulation time is also adequate because the structures of the model systems, especially the distribution of water molecules, were confirmed to be stable after equilibration and data sampled in the last 5 ns were used for the analysis. Thus our model systems meet the requirements for analyzing the motion of water molecules and are not intended to be used to study the motion of objects with a large molecular mass or to visualize physical phenomena related to dynamic changes in the morphology of the membranes. In this study, we only needed to prepare several kinds of model

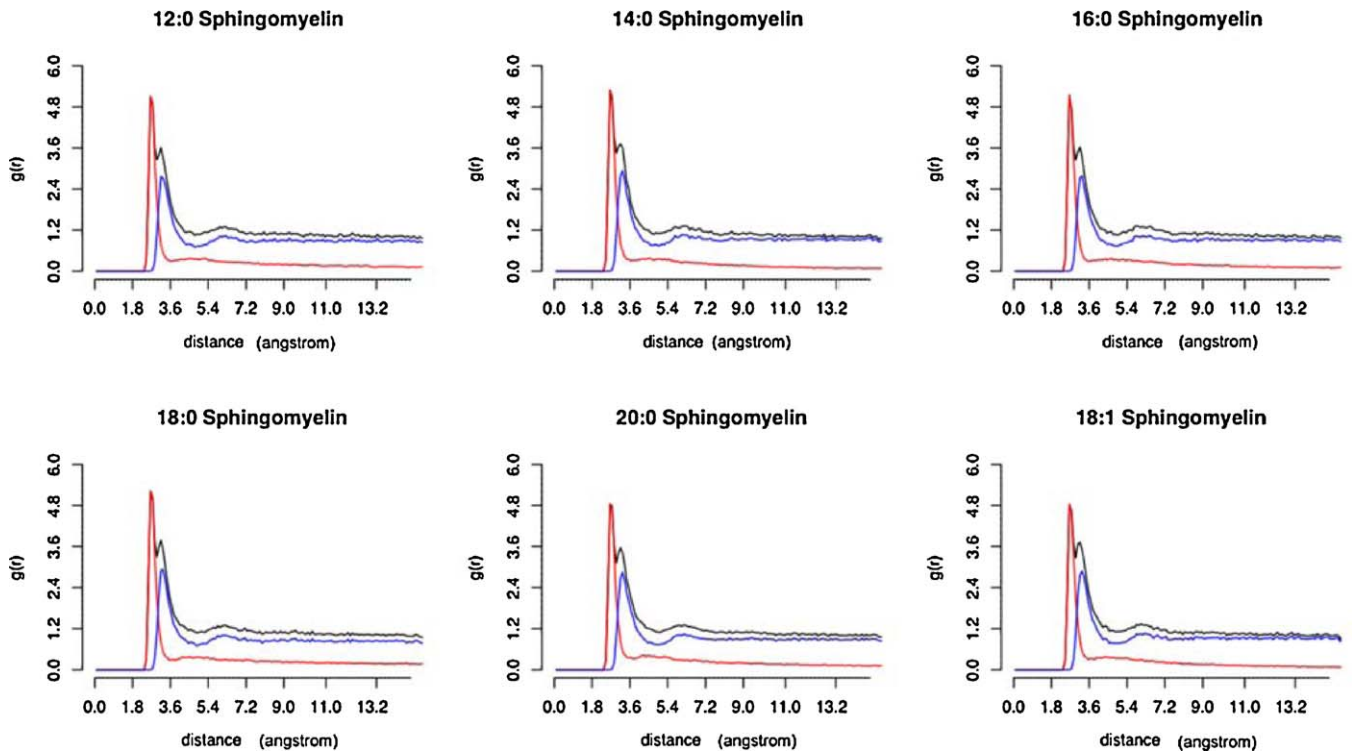

Fig. 5. Distribution function of water molecules on the sphingomyelin membranes. The total distribution function (black) is composed of the water molecules whose closest lipid atom is oxygen (red) and those whose closest lipid atom is carbon (blue). (For interpretation of the references to color in this figure legend, the reader is referred to the web version of the article.)

systems to observe reproducibility within a lipid family and to clarify the trend with the increase of the carbon chain length because characterization of water residence was our main purpose.

4.4. Basic data profile and gauche ratio

Determining the fundamental properties of materials is one of the important roles of computational chemistry, and comparing the data from simulations with those from experiments is critical for assessing the reliability of the simulations. There is, however, quite little experimental data that directly corresponds with the present simulation. In this work, we measured the thickness, area per lipid, gauche ratio and order parameter for the membranes as the basic data. Some previous X-ray analysis data by Shah et al. showed that the lamella periodic length of a 16:0 ceramide crystal is 41.8 Å [45], consistent with our calculated thickness in Table 1.

As for other theoretical calculations, Padit and Scot performed simulations of a 16:0 ceramide bilayer in the liquid crystalline phase at 368 K [4]. In their simulation, the area per lipid was calculated to be 55.1 Å^2, compatible with our area per lipid for the 18:1 ceramide bilayer in the liquid crystalline phase, 54.9 Å^2 in Table 1.

Among the fundamental data, the gauche conformation needs to be given careful attention. The gauche ratio cannot be concretely defined for our computer simulations because none of the angles are precisely $\pm 120^\circ$ and because the gauche conformation is defined on sp^3 carbon and not usually applied to unsaturated lipids. The gauche ratio is often discussed when the phase state of a membrane, such as a gel or liquid crystal phase, is to be determined in experiments. The ratio of the distance of a carbon chain of each lipid compared to the distance when the carbon chain is in the straight form and the angle made by two vectors aligned with the ends of the respective carbon chains of the lipid can be used to distinguish membrane phases in molecular dynamics simulations. We tested this method of analysis and successfully separated gel and liquid crystalline phases, as shown in Fig. S10.

5. Conclusion

Molecular dynamics simulations were performed for ceramide and sphingomyelin lipid bilayers with the carbon chain lengths of the acyl group varied between 12 and 20. Fundamental properties of the membranes—thickness, area per lipid, and gauche ratio—were obtained for each lipid bilayer. Based on the geometry of the molecules appearing in the simulation, the distribution function of water was obtained as a function of distance to the surface along the normal to the membrane. The residence time of water on the membrane's surface was estimated from the potential of the mean force field derived from the distribution function. The water residence time was calculated to be about 6 ps for the ceramide bilayers with saturated acyl groups, while the time was 8–9 ps for the sphingomyelin bilayers. This difference indicates that a sphingomyelin membrane is capable of retaining water molecules longer than a ceramide membrane. The simulation further indicates that the incorporation of unsaturated carbon chains makes the water residence time shorter both in the ceramide and sphingomyelin. These findings point to the significance of the molecular structure of a membrane surface for water retention.

Acknowledgements

This work is supported by a grant from the Japanese Society for the Promotion of Science. One of the authors, X. L., is supported by a Japanese Society for the Promotion of Science (JSPS) research fellowship for foreign researchers. Part of this work was performed at the Research Center for Computational Science, Okazaki, Japan, and the Information Technology Center of the University of Tokyo, and on the high-performance computer system at the Institute for Media Information Technology at Chiba University.

Appendix A. Supplementary data

Supplementary data associated with this article can be found, in the online version, at doi:10.1016/j.jmgm.2010.09.002.

References

[1] M. Sega, P. Brocca, S. Melchionna, R. Vallauri, J. Phys. Chem. B 108 (2004) 20322–20330.
[2] D. Roy, C. Mukhopadhyay, J. Biomol. Struct. Dyn. 19 (2002) 1121–1132.
[3] A. Anishkin, S. Sukharev, M. Colombini, Biophys. J. 90 (2006) 2414–2426.
[4] S.A. Pandit, H.L. Scott, J. Chem. Phys. 124 (2006) 014708.
[5] M. Alexander, A.M. Smondyrev, M.L. Berkowitz, Biophys. J. 76 (1999) 2472–2478.
[6] S.A. Pandit, E. Jakobsson, H.L. Scott, Biophys. J. 87 (2004) 3312–3322.
[7] M. Bachar, O.M. Becker, Biophys. J. 78 (2000) 1359–1375.
[8] P.D. Blood, G.A. Voth, Proc. Natl. Acad. Sci. U.S.A. 103 (2006) 15068–15072.
[9] R.O. Dror, D.H. Arlow, D.W. Borhani, M.Ø. Jensen, S. Piana, D.E. Shaw, Proc. Natl. Acad. Sci. U.S.A. 106 (2009) 4689–4694.
[10] F. Schotte, J. Soman, J.S. Olson, M. Wulff, P.A. Anfinrud, J. Struct. Biol. 147 (2004) 235–246.
[11] F. Hirata, K. Arakawa, Bull. Chem. Soc. Jpn. 46 (1973) 3367–3369.
[12] S.H. Chong, F. Hirata, J. Phys. Chem. B 101 (1997) 3209–3220.
[13] N. Agmon, E. Pines, D. Huppert, J. Chem. Phys. 88 (1988) 5631–5638.
[14] R.W. Impey, P.A. Madden, I.R. McDonald, J. Phys. Chem. 87 (1983) 5071–5083.
[15] S. Obst, H. Bradaczek, J. Phys. Chem. 100 (1996) 15677–15687.
[16] D. Laage, J.T. Hynes, J. Phys. Chem. B 112 (2008) 7697–7701.
[17] S. Hakomori, Y. Igarashi, J. Biochem. 118 (1995) 1091–1103.
[18] K. Simons, E. Ikonen, Nature 387 (1997) 569–572.
[19] K. Simons, W.L. Vaz, Annu. Rev. Biophys. Biomol. Struct. 33 (2004) 269–295.
[20] Megha, E. London, J. Biol. Chem. 279 (2004) 9997–10004.
[21] L.M. Obeid, C.M. Linardic, L.A. Karolak, Y.A. Hannun, Science 259 (1993) 1769–1771.
[22] Y.A. Hannun, Science 274 (1996) 1855–1859.
[23] Y.A. Hannun, L.M. Obeid, J. Biol. Chem. 277 (2002) 25847–25850.
[24] A.D. Nardo, P. Wertz, A. Giannetti, S. Seidenari, Acta Derm. Venereol. 78 (1998) 27–30.
[25] G. Imokawa, A. Akihito, K. Jin, Y. Higaki, M. Kawashima, A. Hidano, J. Invest. Dermatol. 96 (1991) 523–526.
[26] A. Yamamoto, S. Serizawa, M. Ito, Y. Sato, Arch. Dermatol. Res. 283 (1991) 219–223.
[27] H. Chen, R. Mendelsohn, M.E. Rerek, D. Moore, J. Biochim. Biophys. Acta 1468 (2000) 293–303.
[28] L. Li, X. Tang, K.G. Taylor, D.B. DuPre, M.C. Yappert, Biophys. J. 82 (2002) 2067–2080.
[29] J. Yamagishi, Y. Imai, K. Mori, M. Suzuki, S. Neya, T. Hoshino, e-J. Surf. Sci. Nanotech. 7 (2009) 591–595.
[30] W. Humphrey, A. Dalke, K. Schulten, J. Mol. Graph. 14 (1996) 33–38.
[31] W.L. Jorgensen, J. Chandrasekhar, J.D. Madura, R.W. Impey, M.L. Klein, J. Chem Phys. 79 (1983) 926–935.
[32] J.C. Phillips, R. Braun, W. Wang, J. Gumbart, E. Tajkhorshid, E. Villa, C. Chipot, R.D. Skeel, L. Kale, K. Schulten, J. Comput. Chem. 26 (2005) 1781–1802.
[33] S.E. Feller, A.D. MacKerell, J. Phys. Chem. B 104 (2000) 7510–7515.
[34] A.D. MacKerell, D. Bashford, M. Bellott, R.L. Dunbrack, J.D. Evanseck, M.J. Field, S. Fischer, J. Gao, H. Guo, S. Ha, et al., J. Phys. Chem. B 102 (1998) 3586–3616.
[35] U. Essmann, L. Perera, M.L. Berkowitz, T. Darden, H. Lee, L.G. Pedersen, J. Chem. Phys. 103 (1995) 8577–8593.
[36] M.P. Allen, D.J. Tildesley, Computer Simulation of Liquids, Oxford University Press, New York, 1989.
[37] S. Miyamoto, P.A. Kollmun, J. Comput. Chem. 13 (1992) 952–962.
[38] S.E. Feller, Y. Zhang, R.W. Pastor, B.R. Brooks, J. Chem. Phys. 103 (1995) 4613–4621.
[39] T. Zaraiskaya, K.R. Jeffrey, Biophys. J. 88 (2005) 4017–4031.
[40] D.E. Moilanen, D. Wong, D.E. Rosenfeld, E.E. Fenn, M.D. Fayer, Proc. Natl. Acad. Sci. U.S.A. 106 (2009) 375–380.
[41] H.J. Bakker, Nat. Chem. 1 (2009) 24.
[42] S.W. Chiu, S. Vasudevan, E. Jakobsson, R.J. Mashl, H.L. Scott, Biophys. J. 85 (2003) 3624–3635.
[43] Y. Takaoka, H. Miyagawa, K. Kitamura, Fluid Phase Equilib. 144 (1998) 387–393.
[44] M. Patra, M. Karttunen, M.T. Hyvönen, E. Falck, P. Lindqvist, I. Vattulainen, Biophys. J. 84 (2003) 3636–3645.
[45] J. Shah, J.M. Atienza, R.I. Duclos, A.V. Rawlings, Z. Dong, G.G. Shipley, J. Lip. Res. 36 (1995) 1936–1944.